Analytical Methods

Accepted Manuscript

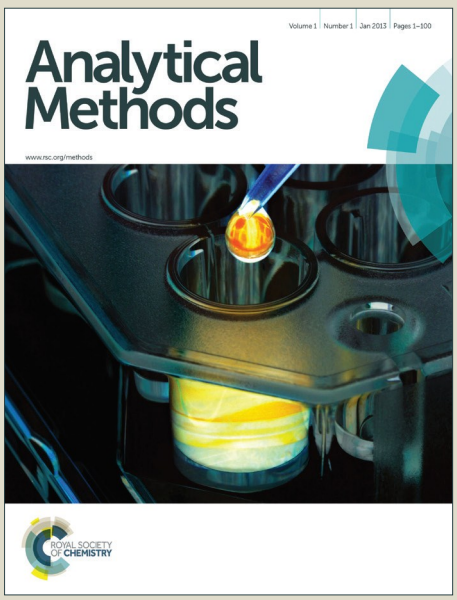

This is an *Accepted Manuscript*, which has been through the Royal Society of Chemistry peer review process and has been accepted for publication.

Accepted Manuscripts are published online shortly after acceptance, before technical editing, formatting and proof reading. Using this free service, authors can make their results available to the community, in citable form, before we publish the edited article. We will replace this *Accepted Manuscript* with the edited and formatted *Advance Article* as soon as it is available.

You can find more information about *Accepted Manuscripts* in the Information for Authors.

Please note that technical editing may introduce minor changes to the text and/or graphics, which may alter content. The journal's standard Terms & Conditions and the Ethical guidelines still apply. In no event shall the Royal Society of Chemistry be held responsible for any errors or omissions in this *Accepted Manuscript* or any consequences arising from the use of any information it contains.

ROYAL SOCIETY OF CHEMISTRY

www.rsc.org/methods

Characterization of Firearms Discharge Residue Recovered from Skin Swabs using Sub-micrometric Mass Spectrometry Imaging

Anthony Castellanos[1], Suzanne Bell[2], and Francisco Fernandez-Lima[1,3*]

[1] Department of Chemistry and Biochemistry, Florida International University, Miami, FL 33199

[2] C. Eugene Bennett Department of Chemistry and the Department Forensic and Investigative Sciences, West Virginia University, 1600 University Avenue, Oglebay Hall Room 208, Morgantown, WV 26506

[3] Biomolecular Science Institute, Florida International University, Miami, FL 33199

Abstract

In the present work, we show the advantages of high spatial resolution interrogation of firearm discharge residues from skin swabs using ion bombardment coupled to mass spectrometry. In particular, the collection of secondary ion and electron maps permitted the chemical (organic and inorganic) and morphological characterization of particulates and organic compounds characteristic to gunshot residues (GSR). Mass spectrometry imaging (MSI) permitted the characterization, at the nanometer level (~300nm resolution), of the composition of particulates and organic compounds from skin swabs. The observation of “consistent” and “characteristic” inorganic compounds (e.g., Sb-Pb-Ba) from single particulates permitted the unambiguous identification of GSR from the skin swabs. In addition, the observation of characteristic secondary ions of nitroglycerin, nitrocellulose, ethyl centralite, dioctyl sulphosuccinate, and dibutyl phthalate suggested the presence of organic gunshot residue (OGSR). That is, our results demonstrate that MSI-TOF-SIMS permits the analysis of skin swabs containing GSR (or not) and OGSR without the need for sample preparation and with little to no damage to the surface of the skin swab (thus preserving the evidence for further analysis).

Key Words: Gunshot residue (GSR), Organic gunshot residue (OGSR), Mass spectrometry imaging (MSI), and Secondary ion mass spectrometry (SIMS).

1. Introduction

When a firearm is discharged, the residue created contains vapors and particles consisting of inorganic particulates (gunshot residue, GSR) originating from the primer, propellant, cartridge and the weapon itself as well as organic components (organic gunshot residue, OGSR) originating from the propellant and firearm lubricants. Main challenges during the analysis of the firearm event (e.g., identification of shooter) reside on the collection, characterization and preservation of the physical and chemical evidence. For example, the firearm discharge residues have been traditionally analyzed by characterizing the GSR via scanning electron microscopy electron dispersive x-ray spectroscopy (SEM/EDS) [1]. Recently, microbeam Ion Beam Analysis (e.g., μ-PIXE) has been reported to provide elemental quantitative and more sensitive determination of "characteristic" GSR species. [2] IBA has also shown promise in detecting smaller elements such as B and Na and has higher sensitivity for Fe than SEM/EDS. [2, 3] Nevertheless, the recent introduction of "green primers" has triggered the screening for OGSR as a way to identify and characterize the chemical evidence. [4, 5] While current analytical efforts are compartmentalized for GSR and OGSR analysis [4, 5], recent studies have shown the advantages of using multiple assays and complementary techniques for the characterization of GSR and OGSR during a firearm discharge (e.g., ATR-FTIR [6], micro-Raman combined with laser ablation ICP-MS [7, 8], LIBS/ICP-OES and GC/μ-ECD and GC/MS [9, 10], SEM/EDS and LC-MS/MS [11-13], SEM/EDS and IBA/μPIXE [2, 3] and TOF-SIMS [14-18]). Recent applications of mass spectrometry to GSR and organic GSR were recently reviewed.[5] The next logical extension of this line of work is to develop methods that allow for simultaneous detection of GSR and OGSR using a single analytical method while preserving the physical and chemical evidence.

Mass spectrometry imaging (MSI) is rapidly becoming the method of choice for chemical mapping of organic and inorganic compounds from surfaces[19-23]. For example, MSI permits the simultaneous interrogation of surfaces with high sensitivity and without the need for labels or pre-selection of molecules of interest; in imaging MS, most if not

all inorganic/organic components can be sampled and detected simultaneously. MSI lateral resolution is ultimately defined by the dimensions of the desorption probe (from tens of nanometers to hundreds of micrometers)[24-26]. The physical dimensions of the firearm discharge particulates (e.g., from few to tens of microns) and the desirability to preserve the sample demands the use of high spatial resolution probes capable of generating characteristic inorganic and organic ions, with little to no sample preparation, for the GSR and OGSR characterization in a single analysis, respectively.

In the present work, we show for the first time the advantages of using high-spatial spatial resolution MSI for the interrogation of surfaces containing GSR and OGSR. In particular, secondary electrons and secondary atomic/molecular ion maps were obtained from a single analysis with small damage to the physical and chemical surface integrity, thus allowing for secondary interrogation of the sample. Typical inorganic and organic molecular ions are described from skin swabs of shooters after a firearm is discharged. The high spatial resolution MSI permitted the identification of GSR and OGSR components based on their spatial distribution using unsupervised PCA analysis. The goal of this work was to demonstrate the capabilities of high resolution MSI combining secondary electron and secondary ion images in order to characterize the firearm discharge skin swabs based on the morphology and composition of the collected species (i.e., particulates and organic compounds).

2. Materials and Methods

2.1 Sample Collection, Preparation and Storage

Samples were prepared by wiping the surface of a shooter's hand with Nomex®/Kevlar® swabs immediately after firing two rounds from a Glock 9mm Model 19 semiautomatic pistol using factory-prepared commercial ammunition. Informed consent was obtained from all volunteers of this study. Swabs were selected to ensure good sampling efficiency of OGSR. Alternatively, stubs can also be tilized to improve sampling of both OGSR and GSR despite the loss of tackiness over large areas. [27] The shooter's hands were cleaned between firing and sampling events with isopropanol. Prior collection, the Nomex®/Kevlar® swabs were pre-moistened with a few mL of isopropanol. Although other solvents may be better suited for optimal one-step

extractions, isopropanol is considered to be an adequate solvent for extraction of volatiles for mass spectrometry. [28, 29] After collections, the swabs were immediately placed in a plastic petri dish, sampled side up, which was taped shut for transportation to the laboratory. Prior to MSI analysis, swabs were cut to 1X1 cm^2 sizes and mounted on the sample stage. A negative control swab and three firearm discharge swabs were analyzed.

2.2 Mass Spectrometry Imaging

Mass spectrometry imaging experiments were performed utilizing a TOF SIMS[5] instrument (ION-TOF, Münster, Germany) retrofitted with a liquid metal ion gun analytical beam for high spatial resolution (25 keV Bi_3^+) and an electron flood gun to reduce surface charging during mass spectrometry analysis. The TOF-SIMS instrument was operated in spectral ("high current bunched", HCBU) and imaging ("burst alignment", BA) modes as described previously.[30-32] The tradeoff between the two modes is the mass resolving power, spatial resolution and secondary ion collection efficiency. Two dimensional secondary electrons and ion maps were collected by rastering the primary 25 keV Bi_3^+ beam over the field of view of interest (typically 100x100 or 150x150 μm^2). In spectral HCBU mode, mass spectra were collected in positive and negative mode with a typical spatial resolution of 1.2 µm, a mass resolving power of $m/\Delta m$= ~5,000 at m/z = 400 and total ion dose ~$5x10^{12}$ ion/cm^2. The imaging BA mode provides a higher spatial resolution (~300 nm) and nominal mass resolution ($m/\Delta m$= ~200) and spectra were collected with a typical total ion doses of ~$5x10^{12}$ ions/cm^2. Replicate measurements (n = 3) were performed on each 1X1 cm^2 swabs. 2D TOF-SIMS data processing and principal component analysis (PCA) were performed using SurfaceLab 6 software (ION-TOF, Münster, Germany). More details on PCA of MSI data can be found elsewhere.[33] All mass spectra were internally calibrated.

3. Results and Discussion

Optical inspection of the firearm discharge swabs showed the presence of multiple particulates of varying size (typically, few to tens of µm), in good agreement with previously reported SEM/EDX results.[34] Most of the particulates were dispersed

(typically hundreds of micrometers apart) and distributed near the surface of the swab material. Closer inspection with the imaging BA TOF-SIMS mode permitted the generation of secondary ion and electron maps with sub-micrometer spatial resolution (see Figure 1). The obtained maps are comparable to previously reported SEM/EDS maps of GSR particles and at least 10-fold higher spatial resolution to previously reported TOF-SIMS maps.[16] The higher spatial resolution of current analysis results from the use of a better focusing primary ion column and the use of the electron flood gun to reduce surface charging. When the same field of view was analyzed in spectral HCBU mode, a near micrometric spatial resolution was obtained while allowing for high mass resolution detection of the secondary ions (see Figure 2).

The high mass resolution permitted the separation of multiple *m/z* signals at the level of nominal mass, and when the chemical maps were submitted to unsupervised principal components analysis, the compartmentalized nature of the GSR and OGSR in terms of spatial distribution resulted in the natural separation of components from the GSR particulate (PC2, 19%) and other components (mostly organics and OGSR) from the swab surface (PC1, 78%). Closer inspection to the *m/z* of the PC1 and PC2 loadings permitted the assignment of chemical formulas from characteristic signals from the GSR and OGSR (see Figure 3 and Table 1). The PC2 loadings showed the distribution of several inorganic compounds: Na^+, K^+, Si^+, Sb^+, Pb^+, $BaCl_2H^+$, BaO_2^+, $(BaO)_{n=0-2}Ba^+$, $(BaO)_{n=1-3}H^+$, $(BaO)_{n=1-2}OH^+$ and $(BaO)_{n=0-2}Sb^+$ in positive ion mode. Closer inspection to the *m/z* distribution showed a good agreement between the theoretical isotopic distributions of the inorganic compounds with the observed experimental distributions. In addition, secondary confirmation of the PC2 loadings was performed by looking at the summed spectra over a small area from the particulate (see Figure 3C) and similar results were obtained. The $(BaO)_{n=0-2}Ba^+$, $(BaO)_{n=1-3}H^+$ and $(BaO)_{n=1-2}OH^+$ series are commonly considered as “consistent” with GSR while the observation of Sb^+, Pb^+ and the $(BaO)_{n=0-2}Sb^+$ series (Sb-Pb-Ba) from a single particulate is considered “characteristic” of GSR.[1] Inspection of the negative spectral HCBU mode showed the presence of characteristic inorganic peaks of GSR (e.g., SbC^-, $SbO_{n=0-2}^-$, Pb^- and $PbOH^-$, see supporting information Figure S1). The analysis of the

PC1 loadings permitted the observation of organic components coming from the swab surface excluding the particulates.

The higher complexity of the *m/z* distribution observed in the PC1 is a consequence of the observation of characteristic ions from the swab as well as the collected OGSR from the shooter's skin. A comparison between the negative control swab and the three samples permitted the identification of potential candidates for OGSR in PC1. Despite the fact that all organic compounds found in ammunition can potentially contribute to the OGSR content found during shooter's swabs, it has been reported that the major observed components originates from propellant powder.[4] Smokeless powders consist predominantly of nitrocellulose (NC) combined with other explosive compounds and additives. These additives include stabilizers, plasticizers, flash inhibitors, coolants, moderants, surface lubricants, and antiwear additives. Some compounds detected after shooting are components of the smokeless powder (i.e., nitroglycerine, dinitrotoluene, stabilizers, additives, etc.), while others are produced during the shooting at a very high temperature and pressure.[10, 13] The molecular structure of these compounds can vary, which is an important consideration when choosing a suitable ionization technique. That is, in contrast to atmospheric pressure ionization sources, the mechanism of secondary ion emission in TOF-SIMS is strongly related to the projectile size and energy.[35-39] For example, the observation of molecular ion and characteristic fragments is directly related to the structure of the molecule of interest.[15, 40, 41] This was considered into the selection of the analysis mode (positive vs negative) and on the candidate assignment by looking at characteristic secondary ions previously identified during the analysis of individual OGSR standards. [15] For example, inspection of PC1 loadings from the three analyzed samples compared to the negative control swab suggested the presence of characteristic molecular ions of nitroglycerin (*m/z* = 165.01), nitrocellulose (*m/z* = 129.05, 113.06, 85.03, 71.01, 69.03 and 57.03), ethyl centralite (*m/z*= 148.08 and 120.08), dioctyl sulphosuccinate (*m/z*= 125.94), dibutyl phthalate (*m/z*= 149.02 and 105.03) and a series of hydrocarbons. These observations of common characteristic fragments between the species proposed have also been observed during the TOF-SIMS analysis of gun powder. [15] While several other OGSR components have been identified (e.g, nitroguanidine, octagon, cyclonite,

diphenylamine, 2,4-dinitrotoluene, etc.), analysis of pure standards using SIMS ionization has yet to be reported. [13] Previously detected more volatile OGSR compounds using SPME GC-MS were not observed during the TOF-SIMS analysis. In addition, while TOF-SIMS provides low detection limits for the analysis of firearm gunshot residue [14-18], the possibility of having isomeric interferences at the *m/z* of interest during the analysis of real samples can increase the complexity during the chemical formula assignment. Nevertheless, when combined with high resolution MSI as previously shown, the number of potential candidates that are typically observed at the level of individual pixels in the surface of the swab is typically reduced to a shorter number of candidate structures.

4. Conclusion

The analysis of firearm gunshot residue from shooter's skin swabs using MSI-TOF-SIMS showed the presence of GSR and OGSR in a single analysis. The collection of secondary electron and secondary ion chemical maps with submicron spatial resolution showed the possibility to detect GSR based on the morphology and composition (multiple inorganic series containing "characteristic" inorganic elements) as those obtained using SEM/EDX (current gold standard for GSR analysis). In addition, the possibility to simultaneously identify OGSR compounds based on the detection of characteristic secondary ions was demonstrated from commonly encountered OGSR in skin swabs. Our results showed that when compared to traditional techniques for GSR and OGSR analysis (see Table 2), MSI (in this case via TOF-SIMS) provides chemical (inorganic and organic) and morphological information with little to no damage to the sample. The possibility to preserve the skin swab for further analyses can be proof extremely valuable for forensic applications, since most of the current techniques that provide chemical information of organics are destructive in nature. In the case of the analysis of skin swabs from firing primers containing GSR and OGSR, unambiguous identification of shooters was achieved s using MSI-TOF-SIMS. Potential challenges may exist in the analysis of "green primers" containing fewer metals 'characteristic' of GSR andvolatile OGSR constituents, which may not be amenable to TOF-SIMS analysis; nevertheless, further studies will permit the identification of characteristic

secondary ions for “green primers” that remain stable in swab samples. Alternatively, further developments of the swab surface chemistry will permit the trapping of volatile OGSR for MSI-TOF-SIMS analysis. It is anticipated that MSI will have an increasing role in examining evidence for forensic applications owed to its ability to detect GSR as well as OGSR in a single analysis.

Acknowledgements

AC was fully supported by a NRC-HQ-84-14-G-0040 fellowship. This work was funded in part through a “National Institute of Justice Forensic Technology Center of Excellence” project, award number #2011-DN-BX-K564, RTI International (6-321-0213168) to SB and by the National Institute of General Medical Sciences grant GM106414 to FF-L.

References

1. A. International, *Journal*, 2010, **E1588-10e1**.
2. F. S. Romolo, M. E. Christopher, M. Donghi, L. Ripani, C. Jeynes, R. P. Webb, N. I. Ward, K. J. Kirkby and M. J. Bailey, *Forensic Science International*, 2013, **231**, 219-228.
3. M. E. Christopher, J.-W. Warmenhoeven, F. S. Romolo, M. Donghi, R. P. Webb, C. Jeynes, N. I. Ward, K. J. Kirkby and M. J. Bailey, *Analyst*, 2013, **138**, 4649-4655.
4. O. Dalby, D. Butler and J. W. Birkett, *J Forensic Sci*, 2010, **55**, 924-943.
5. R. V. Taudte, A. Beavis, L. Blanes, N. Cole, P. Doble and C. Roux, *BioMed Research International*, 2014, **2014**, 965403.
6. J. Bueno and I. K. Lednev, *Analytical Chemistry*, 2014, **86**, 3389-3396.
7. Z. Abrego, N. Grijalba, N. Unceta, M. Maguregui, A. Sanchez, A. Fernandez-Isla, M. Aranzazu Goicolea and R. J. Barrio, *Analyst*, 2014, **139**, 6232-6241.
8. J. C. D. Freitas, J. E. S. Sarkis, O. N. Neto and S. B. Viebig, *Journal of forensic sciences*, 2012, **57**, 503-508.
9. A. Tarifa and J. R. Almirall, *Science & justice : journal of the Forensic Science Society*, 2015, **55**, 168-175.
10. C. Weyermann, V. Belaud, F. Riva and F. S. Romolo, *Forensic Science International*, 2009, **186**, 29-35.
11. J. L. Thomas, D. Lincoln and B. R. McCord, *J Forensic Sci*, 2013, **58**, 609-615.
12. D. Laza, B. Nys, J. D. Kinder, A. Kirsch-De Mesmaeker and C. Moucheron, *Journal of forensic sciences*, 2007, **52**, 842-850.
13. S. Benito, Z. Abrego, A. Sánchez, N. Unceta, M. A. Goicolea and R. J. Barrio, *Forensic Science International*, 2015, **246**, 79-85.
14. J. Coumbaros, K. P. Kirkbride, G. Klass and W. Skinner, *Forensic Science International*, 2001, **119**, 72-81.
15. C. M. Mahoney, G. Gillen and A. J. Fahey, *For. Sci Int.*, 2006, **158**, 39-51.
16. M. I. Szynkowska, A. Parczewski, K. Szajdak and J. Rogowski, *Surface and Interface Analysis*, 2013, **45**, 596-600.

17. M. I. Szynkowska, K. Czerski, J. Rogowski, T. Paryjczak and A. Parczewski, *Surface and Interface Analysis*, 2010, **42**, 393-397.
18. M. I. Szynkowska, K. Czerski, J. Grams, T. Paryjczak and A. Parczewski, *Imaging Sci. J.*, 2007, **55**, 180-187.
19. B. Spengler, *Analytical Chemistry*, 2015, **87**, 64-82.
20. A. Nilsson, R. J. A. Goodwin, M. Shariatgorji, T. Vallianatou, P. J. H. Webborn and P. E. Andrén, *Analytical Chemistry*, 2015, **87**, 1437-1455.
21. R. M. A. Heeren, *International Journal of Mass Spectrometry*, 2015, **377**, 672-680.
22. J. D. DeBord, D. F. Smith, C. R. Anderton, R. M. Heeren, L. Pasa-Tolic, R. H. Gomer and F. A. Fernandez-Lima, *Plos One*, 2014, **9**, e99319.
23. C. Wu, A. L. Dill, L. S. Eberlin, R. G. Cooks and D. R. Ifa, *Mass Spectrometry Reviews*, 2013, **32**, 218-243.
24. M. L. Pacholski and N. Winograd, *Chem. Rev.*, 1999, **99**, 2977-3005.
25. V. Pinnick, S. Rajagopalachary, S. V. Verkhoturov, L. Kaledin and E. A. Schweikert, *Analytical Chemistry*, 2008, **80**, 9052-9057.
26. F. A. Fernandez-Lima, M. J. Eller, J. D. DeBord, S. V. Verkhoturov, S. Della-Negra and E. A. Schweikert, *Nucl. Instr. and Meth. in Phys. Res. B*, 2012, **273**, 270-273.
27. R. V. Taudte, C. Roux, L. Blanes, M. Horder, K. P. Kirkbride and A. Beavis, *Analytical and Bioanalytical Chemistry*, 2016, **408**, 2567-2576.
28. N. Song-im, S. Benson and C. Lennard, *Forensic Science International*, 2012, **223**, 136-147.
29. F. S. Romolo, L. Cassioli, S. Grossi, G. Cinelli and M. V. Russo, *Forensic Science International*, 2013, **224**, 96-100.
30. R. N. Sodhi, *Analyst*, 2004, **129**, 483-487.
31. D. Touboul, F. Kollmer, E. Niehuis, A. Brunelle and O. Laprevote, *J Am Soc Mass Spectrom*, 2005, **16**, 1608-1618.
32. A. Brunelle, D. Touboul and O. Laprevote, *J Mass Spectrom*, 2005, **40**, 985-999.
33. B. J. Tyler, G. Rayal and D. G. Castner, *Biomaterials*, 2007, **28**, 2412-2423.
34. F. Saverio Romolo and P. Margot, *Forensic Science International*, 2001, **119**, 195-211.
35. R. D. Harris, W. S. Baker, M. J. Van Stipdonk, R. M. Crooks and E. A. Schweikert, *Rapid Communications in Mass Spectrometry*, 1999, **13**, 1374-1380.
36. E. J. Smiley, N. Winograd and B. J. Garrison, *Analytical Chemistry*, 2006, **79**, 494-499.
37. F. A. Fernandez-Lima, M. J. Eller, S. V. Verkhoturov, S. Della-Negra and E. A. Schweikert, *J. Phys. Chem. Lett.*, 2010, **1**, 3510-3513.
38. F. A. Fernandez-Lima, V. T. Pinnick, S. Della-Negra and E. A. Schweikert, *Surf. Interface Anal.*, 2011, **43**, 53-57.
39. F. A. Fernandez-Lima, M. J. Eller, J. D. deBord, M. J. Levy, S. V. Verkhoturov, S. della-Negra and A. E. Schweikert, *Journal of Physical Chemistry Letters*, 2012, **3**, 337-341.
40. C. M. Mahoney, *Mass Spectrom. Rev.*, 2010, **29**, 247-293.
41. F. A. Fernandez-Lima, J. Post, J. D. DeBord, M. J. Eller, S. V. Verkhoturov, S. Della-Negra, A. S. Woods and E. A. Schweikert, *Analytical Chemistry*, 2011, **83**, 8448-8453.

Figure and Table captions

Figure 1. Typical optical (A), total secondary ion in burst alignment mode MSI-TOF-SIMS (B), and secondary electron (C) maps of firearms discharge residues recovered from skin swabs.

Figure 2. Typical chemical maps (FOV of 100x100 μm^2) from unsupervised principal components analysis using high current bunched mode MSI-TOF-SIMS showing the distribution of OGSR (left, PC1), GSR (middle, PC2) and composite of PC1 and PC2 (right) of firearms discharge residues recovered from skin swabs .

Figure 3. Typical loading plots for A) PC1 (OGSR) and B) PC2 (GSR) obtained from the analysis of the 2D-TOF-SIMS images from high current bunched mode MSI-TOF-SIMS. C) Notice the isotopic mass distribution obtained in spectral HCBU mode and corresponding theoretical profiles (red lines) for typically observed GSR components (e.g., $BaOH^+$, Ba_2O^+, and $BaSbO^+$) from a 15x15 μm^2 region of interest centered on the GSR particle shown in Figure 1 and 2.

Table 1. GSR and OGSR characteristics secondary ions from high current bunched mode MSI-TOF-SIMS analysis.
* the *m/z* of the most abundant isotope is reported.

	Species	Chemical Formula	m/z
GSR	$(BaO)_nBa^+$ (n = 0-2)	Ba^+	137.90
		$(BaO)Ba^+$	291.80
		$(BaO)_2Ba^+$	445.71
	$(BaO)_nH^+$ (n = 1-3)	$(BaO)H^+$	154.91
		$(BaO)_2H^+$	308.81
		$(BaO)_3H^+$	462.71
	$(BaO)_nOH^+$ (n = 2,3)	$(BaO)_2OH^+$	324.80
		$(BaO)_3OH^+$	478.70
	$(BaO)_nSb^+$ (n = 0-2)	Sb^+	120.90
		$(BaO)Sb^+$	274.80
		$(BaO)_2Sb^+$	428.70
	Pb^+	Pb^+	207.98
OGSR	Nitroglycerin	$C_3H_5O_6N_2^+$	165.01
	Nitrocellulose	$C_6H_9O_3^+$	129.05
		$C_6H_9O_2^+$	113.06
		$C_4H_5O_2^+$	85.03
		$C_3H_3O_2^+$	71.01
		$C_4H_5O^+$	69.03
		$C_3H_5O^+$	57.03
	Hydrocarbons	$C_3H_5O^+$	57.03
		$C_4H_7^+$	55.05
		$C_2H_3O^+$	43.02
		$C_3H_5^+$	41.04
		$C_3H_3^+$	39.02

		$C_2H_5^+$	29.04
		CH_2^+	14.02
	Ethyl centralite	$C_6H_5NC_2H_5CO^+$	148.08
		$C_6H_5NC_2H_5^+$	120.08
	Dioctyl sulphosuccinate	$Na_2SO_3^+$	125.94
	Dibutyl phthalate	$C_8H_5O_3^+$	149.02
		$C_6H_5CO^+$	105.03

Table 2. Comparison of typical techniques used to characterize firearm discharge residues.

Technique	**Destructive**	**Chemical Information (Inorganics/Organics)**	**Morphological Information**	**Relative cost**
Colorimetric	Y	Y/Y	N	Low
IMS	Y	N/Y	N	Low
SEM-EDX	N	Y/N	Y	High
IBA (μPIXE)	N	Y/N	Y	High
ICP-AES/MS	Y	Y/N	N	High
MSI-TOF-SIMS	**N**	**Y/Y**	**Y**	**High**

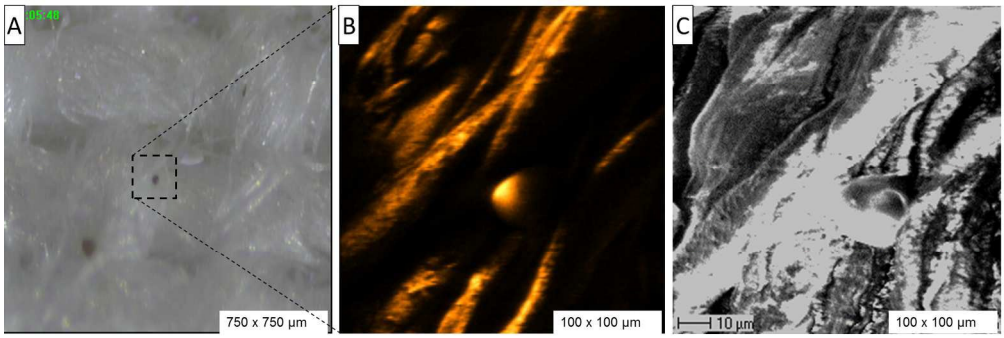

Figure 1
374x125mm (150 x 150 DPI)

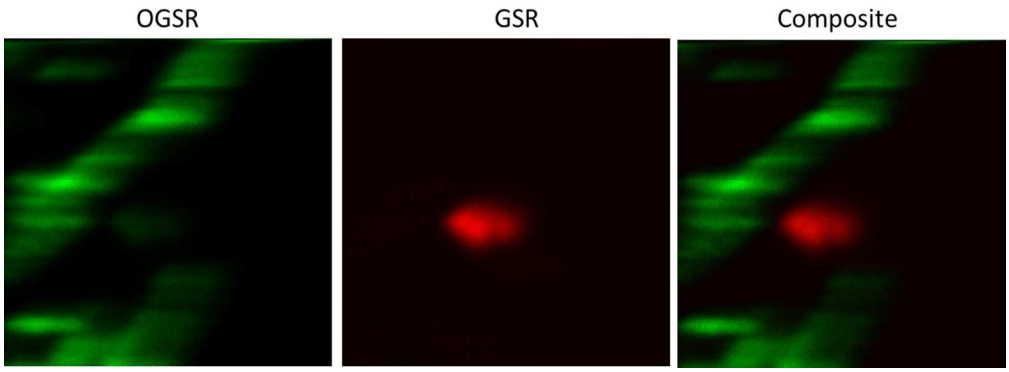

Figure 2
232x87mm (150 x 150 DPI)

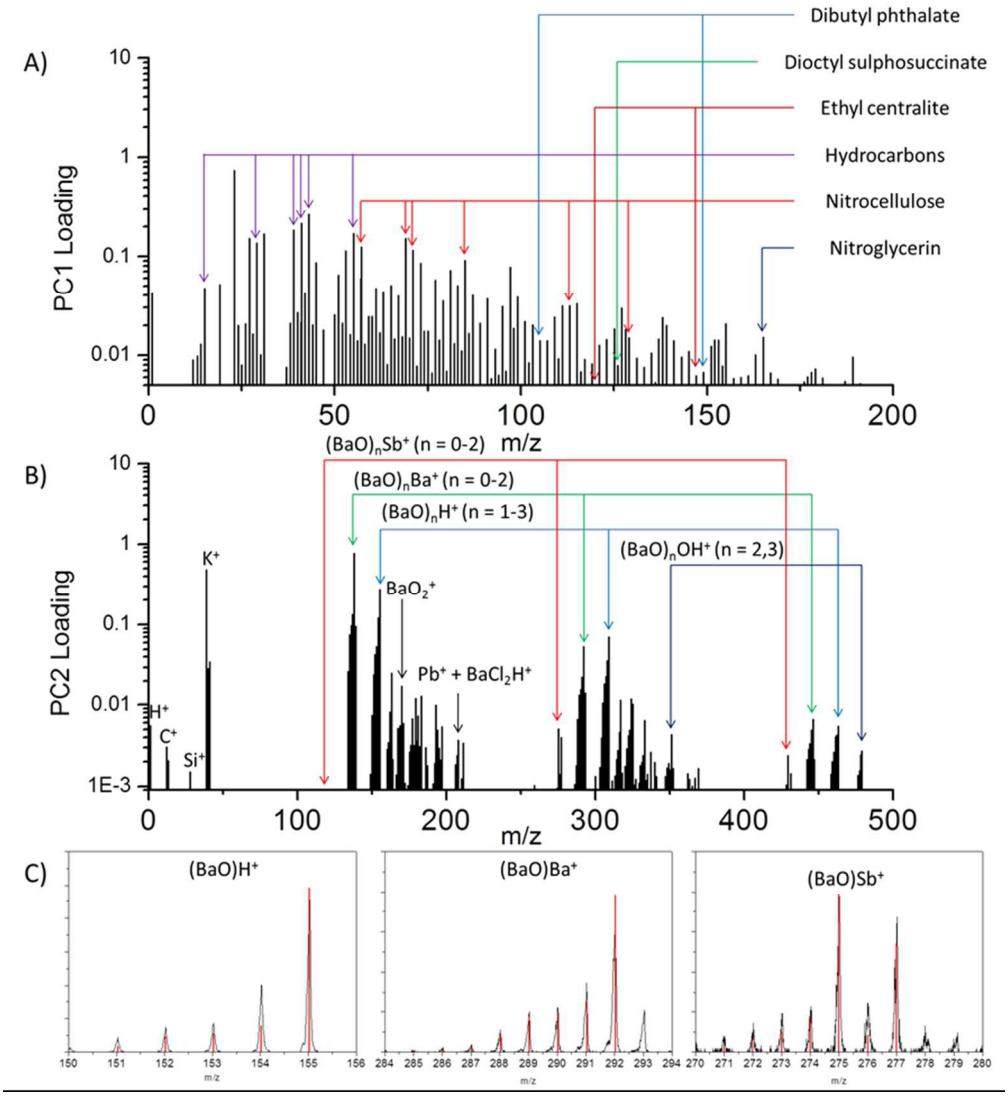

Figure 3

151x165mm (150 x 150 DPI)

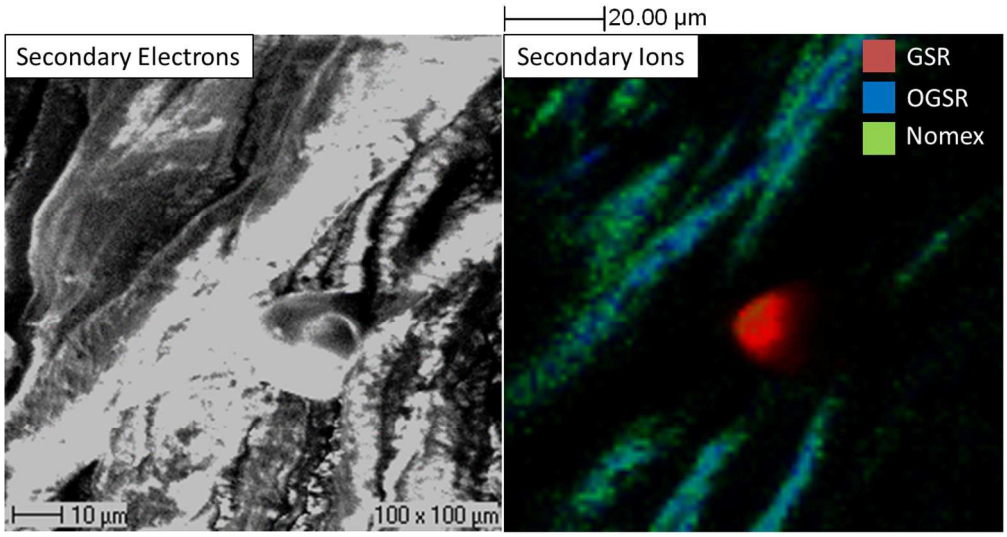

235x124mm (150 x 150 DPI)